Chapter 4
The Delayed van der Pol Oscillator and Energy Harvesting

Check for updates

Zakaria Ghouli, Mustapha Hamdi and Mohamed Belhaq

Abstract In the first part of the chapter, we present some results on quasi-periodic (QP) vibration-based energy harvesting (EH) in a delayed van der Pol oscillator with modulated delay amplitude. Two examples are considered which include a delayed van der Pol harvester coupled either to a delayed or undelayed electromagnetic subsystem. The influence of delay parameters on the performance of the harvester has been examined. It is shown that a maximum amplitude of the response does not induce necessarily a maximum output power. In the second part, we investigate QP vibration-based EH in the case where the van der Pol oscillator is subjected to external harmonic excitation and coupled to a delayed piezoelectric component. Perturbation method is applied near a resonance to obtain approximation of the periodic and QP responses as well as the amplitude of the harvested powers. To guarantee the robustness of the QP vibration during energy extraction operation, a stability analysis is performed and the QP stability chart is determined. Results show that in the presence of time delay in the electrical circuit of the excited van der Pol oscillator, it is possible to harvest energy from QP vibrations with a good performance over a broadband of system parameters away from the resonance. Numerical simulations are conducted to support the analytical predictions.

4.1 Introduction

One of the major goals of using quasi-periodic (QP) vibrations to scavenge energy, usually made away from the resonance, is to improve the stability range and robustness of the energy harvester device which is not always secured when operating in

Z. Ghouli · M. Belhaq (✉)
Faculty of Sciences Ain Chock, University Hassan II Casablanca, Casablanca, Morocco
e-mail: mbelhaq@yahoo.fr

Z. Ghouli
e-mail: ghoulizakaria@gmail.com

M. Hamdi
University Mohammed I Oujda, FST-Al Hoceima, Al-Hoceima, Morocco
e-mail: hamustapha2000@yahoo.fr

the vicinity of the considered resonance. Indeed, when the harvester is operating in the linear regime, its best performance is achieved traditionally at the resonance peak with large-amplitude oscillations. However, such large-amplitude oscillations are obtained only in a narrow region located around the peak, thus limiting considerably the performance of the harvester device; see for instance [1–4]. In the nonlinear regime, on the other hand, energy harvesting (EH) capability can be improved by extending the bandwidth of the harvester over broadband of the excitation frequency. A major inconvenient is that the instability phenomenon induced in the nonlinear frequency response can reduce substantially the system performance when the response is attracted to the low-amplitude motions or when it suffers jump phenomena, as shown in [5]. Thus, the idea emerged from such a limitation is to use the possibility of harvesting energy from vibrations away from the resonance thereby circumventing instabilities. Under certain conditions, QP regime with large amplitude when present away from the resonance may constitute a good candidate.

A simple way to harvest energy in the QP regime away from the resonance is to consider self-induced vibrations represented by limit-cycle (LC) oscillations. Under certain conditions (for instance the presence of additional frequency in the system), the steady-state LC oscillations may lose stability via a secondary Hopf bifurcation producing QP vibrations. However, it is known that the amplitude of such QP vibrations occurring away from the resonance is smaller compared to that of the periodic ones; see for instance [6, 7]. In this case the harvester suffers a substantial reduction in the harvested power indicating that the QP regime should be avoided. For instance, in energy harvester systems subjected to combined aerodynamic and base excitations, it was observed that beyond the flutter speed, the QP response of the harvester leads to a substantial drop of the output power [8, 9]. However, in a recent work by Hamdi and Belhaq [10] it was reported analytically and using numerical simulations that in the delayed van der Pol oscillator with modulated delay amplitude, large-amplitude QP vibrations (larger than the periodic ones) performing in broader range of parameters can take place. This analytical finding has been first exploited by Belhaq and Hamdi [11] to demonstrate the possibility to scavenge energy directly from QP vibrations over a broadband of modulation frequency away from the resonance with a good performance. Later, Ghouli et al. [12] investigated QP vibration-based EH in a forced and delayed Duffing harvester device considering an electromagnetic coupling with time delay [13]. More recently, the problem of QP vibration-based EH in a Mathieu-van der Pol-Duffing MEMS device using time delay was studied in [14]. Other variants on the topic have been examined in [15, 16]. The conclusion emerged from these previous works was that for appropriate values of delay parameters, QP vibration-based EH can be used to extract energy over a broadband of excitation frequencies away from the resonance with good performance, thereby circumventing bistability and jump phenomena near the resonance.

The objective of this work is to provide, in a first part, a review on the main results obtained on the QP vibration-based EH in a van der Pol harvester and then investigate, in a second part, EH in a van der Pol oscillator subject to harmonic excitation and coupled to a delayed piezoelectric mechanism.

The chapter is organized as follows: In Sect. 4.2 we present a review on the recent results on QP vibration-based EH in a van der Pol oscillator with time-periodic delay amplitude coupled either to undelayed electromagnetic component or to delayed electromagnetic one. Section 4.3 investigates QP vibration-based EH in a forced van der Pol oscillator coupled to a delayed piezoelectric element. Approximations of the periodic response and the amplitude of the output power near the primary resonance are given using the multiple scales method. Section 4.4 provides approximation of the QP response and the corresponding harvested power applying the second-step multiple scales method. The influence of time delay parameters in the electrical circuit on the EH performance is analyzed. A summary of the results is given in the concluding section.

4.2 The van der Pol Oscillator and Energy Harvesting

The concept of harvesting energy from QP vibrations is demonstrated in this section through two examples. Namely, a delayed van der Pol oscillator coupled to undelayed or delayed electromagnetic component. First, consider a delayed pure van der Pol oscillator with time-periodic delay amplitude studied by Hamdi and Belhaq [10]. The authors analyzed the influence of the modulated time-delay amplitude on the response of the following van der Pol oscillator with time delay in the position and velocity

$$\ddot{x} + x - \varepsilon(\alpha - \beta x^2)\dot{x} - \varepsilon\lambda(t)x(t - \tau) - \varepsilon\lambda_3\dot{x}(t - \tau) = 0 \qquad (4.1)$$

where ε is a small positive parameter, α, β are damping coefficients, $\lambda(t)$, λ_3 are delay amplitudes in the position and velocity, respectively, and τ is the time delay. An overdot denotes differentiation with respect to time t. Equation (4.1) can model ambient sustained self-excited vibrations under a delayed feedback control. Examples includes, for instance, controlled vibration produced by high speed rotating machines or regenerative effects in cutting processes [17–19]. To generate a resonant condition and guarantee the occurrence of QP vibrations, it was assumed that the delay amplitude in the position $\lambda(t)$ is time-periodic around a nominal value λ_1, such that

$$\lambda(t) = \lambda_1 + \lambda_2 \cos \omega t \qquad (4.2)$$

where λ_2 and ω are the amplitude and the frequency of the modulation. The nominal value λ_1 being the unmodulated delay amplitude. The case of *delay parametric resonance* for which the frequency ω of the modulation is near twice the natural frequency of the oscillator was considered. This resonance imposes the condition $1 = (\frac{\omega}{2})^2 + \varepsilon\sigma$ where σ is the detuning parameter.

The periodic response near this *delay parametric resonance* is approximated using the averaging method [20] and the amplitudes of the QP vibrations are obtained applying the second-step multiple scales method [22].
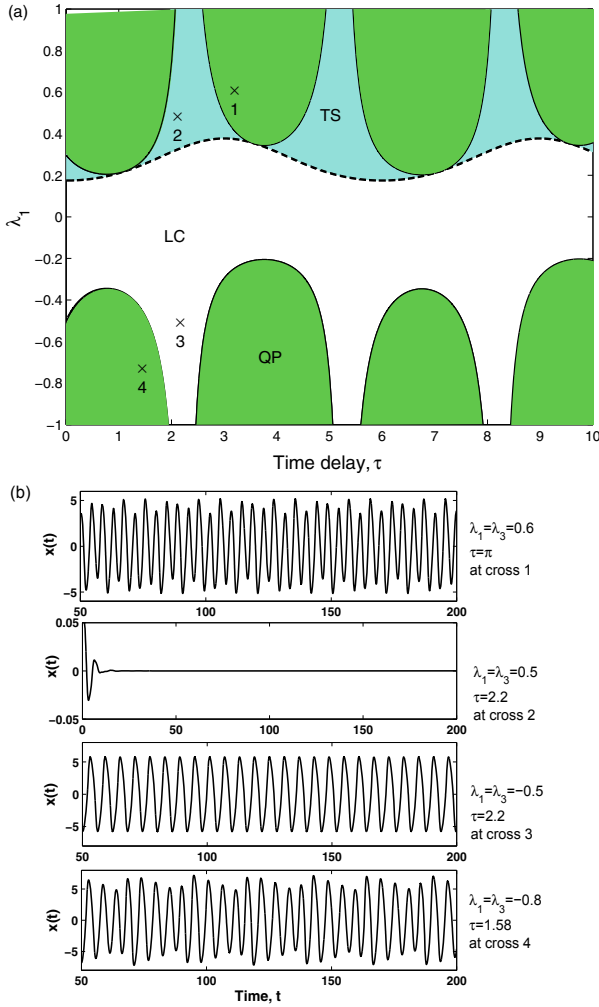
Fig. 4.1 **a** Stability chart of the QP response in the parameter plane (λ_1, τ); $\omega = 2.1$ and $\lambda_2 = 0.8$, LC: Limit cycle, TS: trivial solution, **b** time histories corresponding to different regions [10]

Figure 4.1a provides the stability chart of the QP vibrations in the parameter plane (λ_1, τ) and Fig. 4.1b shows time histories corresponding to different regions of Fig. 4.1a. The transitions of solutions are shown by moving between the crosses 1, 2, 3 and 4 in Fig. 4.1a. For instance, between cross 2 and cross 1 the response of the system undergoes a transition between no oscillation and QP vibration which is a bifurcation of a trivial stable equilibrium point to a stable QP solution. From cross 2 to 3 Hopf bifurcation takes place leading to periodic response and from cross 3 to 4 the solution bifurcates from periodic to QP oscillation, and from cross 3 to 1 similar bifurcation occurs via a secondary Hopf bifurcation.
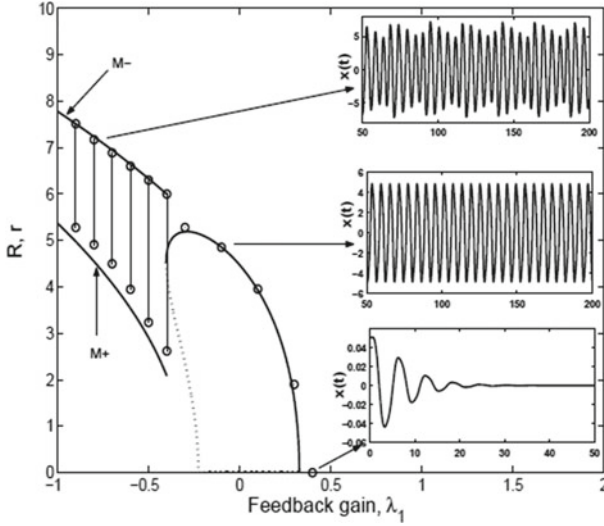
Fig. 4.2 Variation of periodic and QP responses versus λ_1 [10]

In Fig. 4.2 is shown the variation of periodic and QP repones versus λ_1 for $\lambda_3 = \lambda_1$, $\lambda_2 = 0.8$ and $\tau = 1.58$. The QP modulation envelope obtained by numerical simulation (circles) are compared to the analytical prediction (solid lines) for validation. Time series correspond to different regimes are also provided. The main result indicates that the modulation of the delay amplitude in the position gives birth to QP vibrations with large-amplitude performing away from the resonance in the region of negative λ_1.

Taking advantage of this previous finding, its first application to EH has been addressed in Belhaq and Hamdi [11]. They have considered a harvester device consisting in a delayed van der Pol oscillator coupled to an electromagnetic coupling in the form

$$\ddot{x} + x - \varepsilon(\alpha - \beta x^2)\dot{x} = \varepsilon\lambda(t)x(t - \tau) + \varepsilon\gamma_1 i \tag{4.3}$$

$$\frac{di}{dt} + \gamma_2 i = -\dot{z} \tag{4.4}$$

where ε is a small positive parameter, α, β are damping coefficients, $\lambda(t)$ is the delay amplitude, τ is the time delay and γ_1 is the electromagnetic coupling coefficient. The delay amplitude $\lambda(t)$ is assumed to be modulated harmonically as $\lambda(t) = \lambda_1 + \lambda_2 \cos \omega t$, where λ_1 is the unmodulated delay amplitude and λ_2, ω are, respectively, the amplitude and the frequency of the modulation, while i and $\frac{di}{dt}$ have been substituted for electric charge coordinate q ($i = \dot{q}$). The coefficient γ_2 is the reciprocal of the time constant of the electrical circuit. It is worthy to point out that the delay in the mechanical part is not considered as an input power. It should be considered as inherently present in the harvester system as in milling and

turning operations [17–19]. The system response was investigated near the *delay parametric resonance* assumig the resonance condition $1 = (\frac{\omega}{2})^2 + \varepsilon\sigma$ where σ is a detuning parameter. Averaging method was used to approximate the amplitude and the output power of the periodic vibrations and the second-step perturbation method was applied to approximate the amplitude of the QP vibrations and the corresponding output power of the harvester device. For validation, the analytical prediction
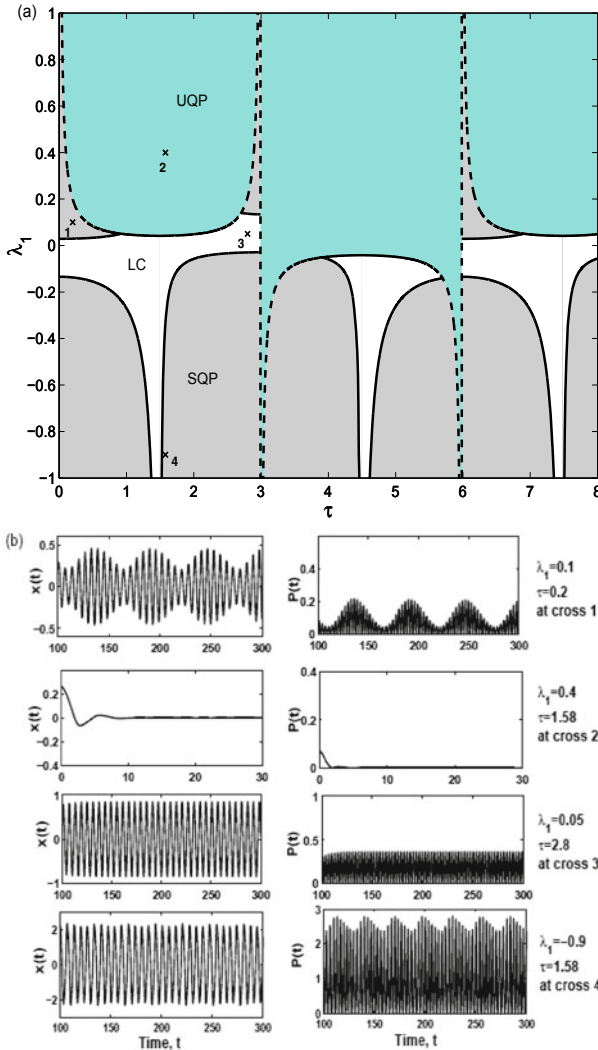

Fig. 4.3 **a** Stability chart of QP solutions in the parameter plane (λ_1, τ), **b** time histories corresponding to different regions; $\lambda_2 = 0.2$, $\omega = 2.1$ and $\gamma_2 = 1.33$. UQP: unstable QP, SQP: stable QP, LC: limit cycle [11]

(solid lines) are compared to numerical simulation (circles) obtained using `dde23` algorithm [21].

In Fig. 4.3a is presented the stability chart of the QP vibrations in the parameter plane (λ_1, τ). Regions of stable and unstable QP vibrations are indicated, respectively, by UQP (aqua regions) and SQP (grey regions). Within the white region periodic oscillations indicated by LC occur. Time histories of responses and powers corresponding to different regions of Fig. 4.3a are shown in Fig. 4.3b. Bifurcation of solutions are obtained by moving between regions in Fig. 4.3a. For instance, from cross 2 to 3 Hopf bifurcation occurs giving rise to LC oscillations. The system behavior changes from LC to SQP oscillation with a slight modulation when moving from
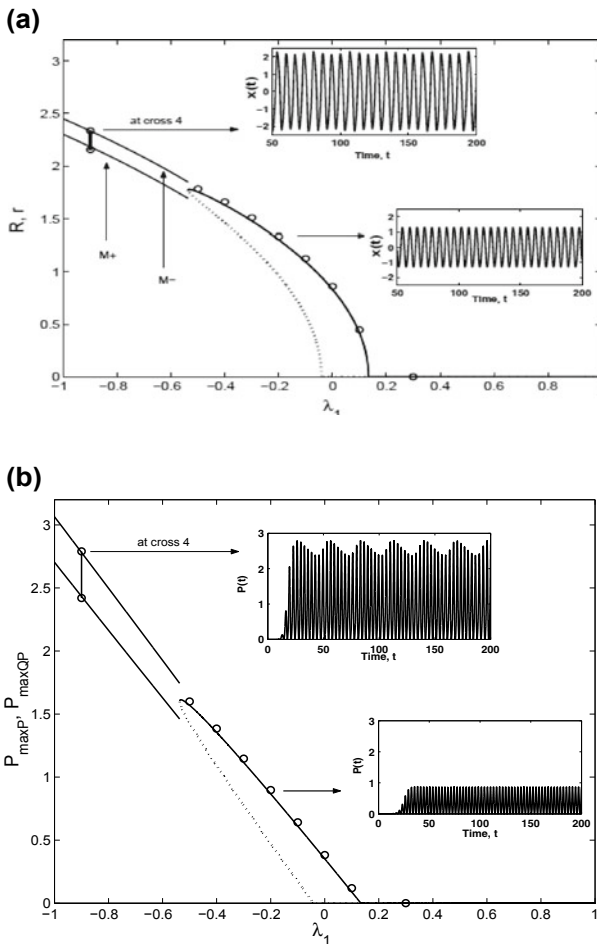

Fig. 4.4 Vibration (**a**) and power (**b**) amplitudes versus λ_1 for $\tau = 1.58$, $\omega = 2.1$ and $\gamma_2 = 1.33$; analytical (solid lines) and numerical (circles) approximations [11]
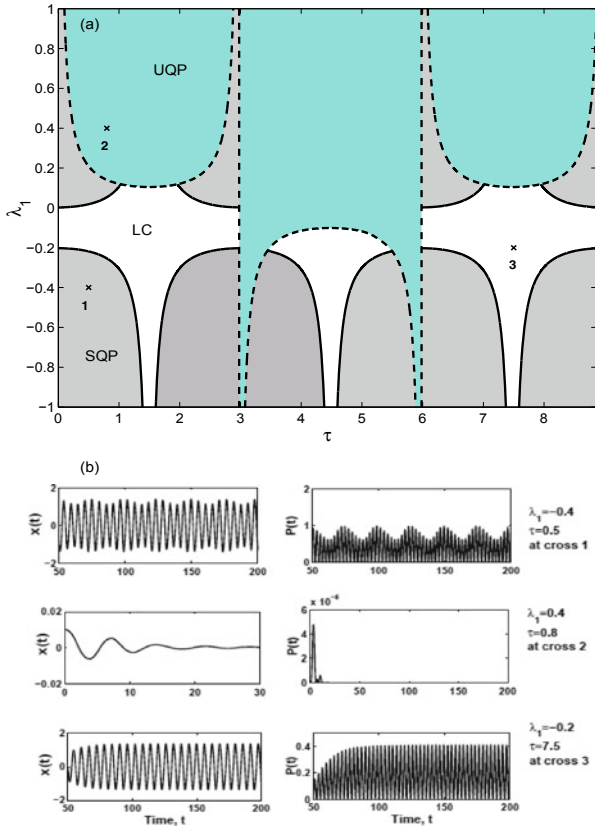
Fig. 4.5 a Stability chart of QP solutions in the plane (λ_1, τ), **b** time histories corresponding to different regions; $\lambda_2 = 0.2$, $\omega = 2.1$ and $K = \gamma_2 = 1.33$. UQP: unstable QP, SQP: stable QP, LC: limit cycle [13]

cross 3 to 4. It is worthy mentioning that cross 4 has been carefully chosen close to the bifurcation curve to demonstrate the accuracy of the analytical prediction of the stability chart. This is illustrated by comparison to time series corresponding to cross 4 in Fig. 4.3a (see Fig. 4.3b bottom).

Figure 4.4 depicts the variation of vibration and power amplitudes versus λ_1. One can clearly observe from Fig. 4.4a that for negative values of λ_1 the amplitude of the QP modulation is larger comparing to the amplitude of the periodic response. Accordingly, the corresponding power amplitudes shown in Fig. 4.4b demonstrate clearly that the performance of the extracted power in the QP region is better than the performance of the output power in the periodic region.

Another case has been considered by Ghouli et al. [13] for which the time delay is introduced in both mechanical and electrical components. In this case, the EH system consists of a delayed van der Pol oscillator coupled to a delayed electromagnetic

Fig. 4.6 Vibration (**a**) and power (**b**) amplitudes versus λ_1 for $\tau = 0.3$, $\lambda_2 = 0.2$, $\omega = 2.1$ and $\gamma_2 = 1.33$; analytical (solid lines) and numerical (circles) approximations. Black line for delayed circuit $K = \gamma_2$, grey line for undelayed circuit $K = 0$. Solid line for stable and doted line for unstable [13]
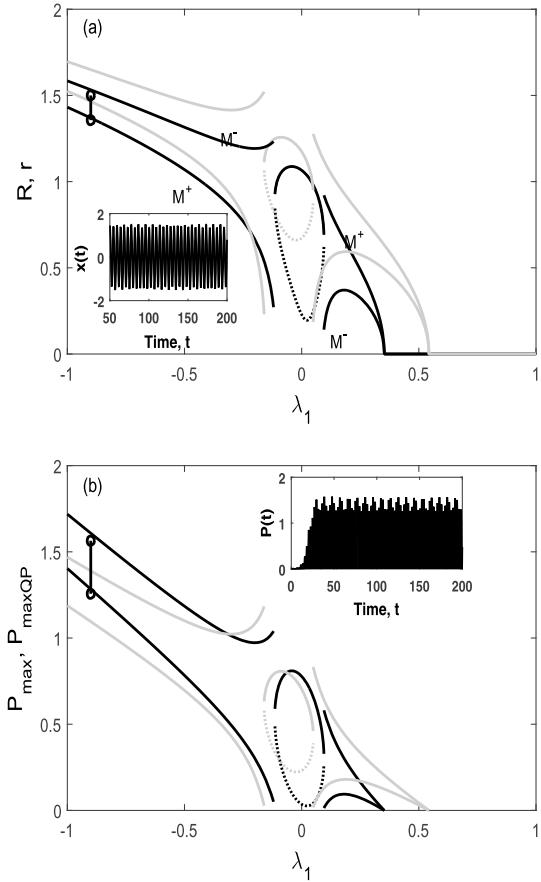
element. The governing equations are written as

$$\ddot{x} + x - \varepsilon(\alpha - \beta x^2)\dot{x} = \varepsilon\lambda(t)x(t - \tau) + \varepsilon\gamma_1 i \tag{4.5}$$

$$\frac{di}{dt} + \gamma_2 i = Ki(t - \tau) - \dot{z} \tag{4.6}$$

where K is the delay amplitude in the electric circuit and τ is the time delay. The other parameters are defined as before.

As in the previous case (4.3), (4.4), the response of the system was investigated near the *delay parametric resonance* using a similar perturbation analysis.

Figure 4.5a presents the stability chart of the QP vibrations in the parameter plane (λ_1, τ). The dashed lines delimit domains of unstable QP vibrations and the solid lines determine the domains where the QP vibrations are stable. Similarly, UQP (*aqua* regions) means unstable QP while SQP (*grey* regions) means stable QP. The

periodic oscillations exist in the *white* regions and are indicated by LC. Time histories and the corresponding output power responses are shown in Fig. 4.5b. The transitions of solutions are obtained by moving between the crosses 1, 2 and 3 in Fig. 4.5a.

Figure 4.6 shows the variation of vibration and power amplitudes versus λ_1 for $K = 0$ (undelayed circuit, *grey* lines) and $K = \gamma_2$ (delayed circuit, *black* lines). It can be seen that negative values of λ_1 decreases the amplitude of the QP modulation (Fig. 4.6a, *black* envelope), but on the contrary, increases the harvested power (Fig. 4.6b, *black* envelope). In other words, in the delayed van der Pol harvester in which the delay is also introduced in the electrical circuit the maximum output power extracted from QP vibration does not necessarily correspond to the maximum amplitude of QP oscillations.

4.3 The Excited van der Pol Oscillator and Energy Harvesting

In this part we study QP vibration-based EH in an excited van der Pol oscillator coupled to a delayed piezoelectric device. The main purpose here is to examine the influence of the time delay in the electrical circuit on the energy extracted from QP vibrations. The corresponding schematic of the harvester is presented in Fig. 4.7 and the governing equations can be written in the dimensionless form as

$$\ddot{x}(t) + x(t) - [\alpha - \beta x(t)^2]\dot{x}(t) - \chi v(t) = f\cos(\omega t) \tag{4.7}$$

$$\dot{v}(t) + \lambda[v(t) - v(t - \tau)] + \kappa\dot{x}(t) = 0 \tag{4.8}$$

where $x(t)$ is the relative displacement of the rigid mass m, α and β are the mechanical damping coefficients, f, ω are, respectively, the amplitude and the frequency of the harmonic excitation, $v(t)$ is the voltage across the load resistance, χ is the piezoelectric coupling term in the mechanical attachment, κ is the piezoelectric coupling term, λ is the reciprocal of the time constant of the electrical circuit and τ is the time delay.

The objective is to investigate periodic and QP responses as well as the corresponding output powers of the harvester device (4.7), (4.8). We perform perturbation method near the principal resonance by introducing the resonance condition $1 = \omega^2 + \sigma$ where σ is a detuning parameter. The first-step multiple scales method is implemented by introducing a bookkeeping parameter ε and scaling parameters such as (4.7) and (4.8) take the form

$$\ddot{x}(t) + \omega^2 x(t) = \varepsilon[(\alpha - \beta x(t)^2)\dot{x}(t) + \chi v(t) + f\cos(\omega t) - \sigma x(t)] \tag{4.9}$$

$$\dot{v}(t) + \lambda[v(t) - v(t - \tau)] + \kappa\dot{x}(t) = 0 \tag{4.10}$$
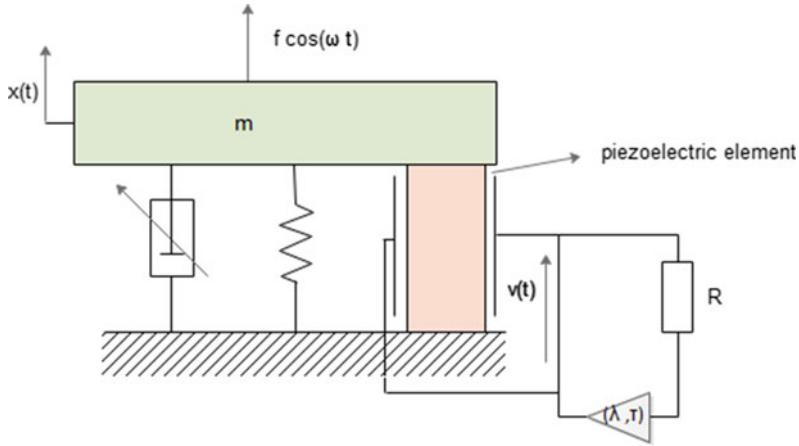
Fig. 4.7 Schematic description of the EH system

A solution to (4.9) and (4.10) can be sought in the form

$$x(t) = x_0(T_0, T_1) + \varepsilon x_1(T_0, T_1) + O(\varepsilon^2) \tag{4.11}$$

$$v(t) = v_0(T_0, T_1) + \varepsilon v_1(T_0, T_1) + O(\varepsilon^2) \tag{4.12}$$

where $T_0 = t$ and $T_1 = \varepsilon t$. The time derivatives become $\frac{d}{dt} = D_0 + \varepsilon D_1 + O(\varepsilon^2)$ and $\frac{d^2}{dt^2} = D_0^2 + \varepsilon^2 D_1^2 + 2\varepsilon D_0 D_1 + O(\varepsilon^2)$ where $D_i^j = \frac{\partial^j}{\partial^j T_i}$. Substituting (4.11) and (4.12) into (4.9) and (4.10) and equating coefficient of like powers of ε, we obtain up to the second order the following hierarchy of problems:

At the first order:

$$D_0^2 x_0 + \omega^2 x_0 = 0 \tag{4.13}$$

$$D_0 v_0 + \lambda[v_0 - v_{0\tau}] + \kappa D_0 x_0 = 0 \tag{4.14}$$

and at the second order:

$$D_0^2 x_1 + \omega^2 x_1 = -2D_0 D_1 x_0 + (\alpha - \beta x_0^2) D_0 x_0 - \sigma x_0 + \chi v_0 + f \cos(\omega t) \tag{4.15}$$

$$D_0 v_1 + \lambda[v_1 - v_{1\tau}] = -D_1 v_0 - \kappa D_0 x_1 - \kappa D_1 x_0 \tag{4.16}$$

Up to the first order the solution is given by

$$x_0(T_0, T_1) = A(T_1)e^{i\omega T_0} + \bar{A}(T_1)e^{-i\omega T_0} \tag{4.17}$$

$$v_0(T_0, T_1) = \frac{-\kappa i\omega A(T_1)}{\lambda + i\omega - \lambda e^{-i\omega\tau}} e^{i\omega T_0} + \frac{\kappa i\omega \bar{A}(T_1)}{\lambda - i\omega - \lambda e^{i\omega\tau}} e^{-i\omega T_0} \tag{4.18}$$

where $A(T_1)$ and $\bar{A}(T_1)$ are unknown complex conjugate functions. Substituting (4.17) and (4.18) into (4.15) and (4.16) and eliminating the secular terms, one obtains

$$-2i\omega(D_1 A) + i\alpha\omega A - i\beta\omega A^2\bar{A} - \sigma A - \frac{\kappa i\omega\chi A}{\lambda + i\omega - \lambda e^{-i\omega\tau}} + \frac{f}{2} = 0 \quad (4.19)$$

Expressing $A = \frac{1}{2}ae^{i\theta}$ where a and θ are the amplitude and the phase, we obtain up to the first order the modulation equations

$$\begin{cases} \dfrac{da}{dt} = S_1 a + S_2 a^3 + S_3\sin(\theta) \\[3mm] a\dfrac{d\theta}{dt} = S_4 a + S_3\cos(\theta) \end{cases} \quad (4.20)$$

where $S_i\,(i = 1, ..., 4)$ are given by

$$S_1 = \frac{\alpha}{2} - \frac{\kappa\chi(\lambda - \lambda\cos(\omega\tau))}{2(\lambda - \lambda\cos(\omega\tau))^2 + 2(\omega + \lambda\sin(\omega\tau))^2}$$

$$S_2 = \frac{-\beta}{8} \qquad S_3 = -\frac{f}{2\omega}$$

$$S_4 = \frac{\sigma}{2\omega} + \frac{\kappa\chi(\omega + \lambda\sin(\omega\tau))}{2(\lambda - \lambda\cos(\omega\tau))^2 + 2(\omega + \lambda\sin(\omega\tau))^2}$$

The solution up to the first order given by (4.17) and (4.18) can be expressed as

$$\begin{cases} x_0(T_0, T_1) = a\cos(\omega t + \theta) \\[3mm] v_0(T_0, T_1) = V\cos\left(\omega t + \theta + \arctan\dfrac{\lambda - \lambda\cos(\omega\tau)}{\omega + \lambda\sin(\omega\tau)}\right) \end{cases} \quad (4.21)$$

such that the condition $\omega + \lambda\sin(\omega\tau) \neq 0$ must be satisfied. Moreover, the voltage amplitude V is given by

$$V = \frac{\kappa\omega}{\sqrt{(\lambda - \lambda\cos(\omega\tau))^2 + (\omega + \lambda\sin(\omega\tau))^2}}a \quad (4.22)$$

The steady-state response of system (4.20), corresponding to periodic solutions of (4.9) and (4.10), are determined by setting $\frac{da}{dt} = \frac{d\theta}{dt} = 0$. Eliminating the phase, we obtain the following algebraic equation in a

$$S_2^2 a^6 + 2S_1 S_2 a^4 + (S_1^2 + S_4^2)a^2 - S_3^2 = 0 \quad (4.23)$$

An expression for the average power is obtained by integrating the dimensionless form of the instantaneous power $P(t) = \lambda v(t)^2$ over a period T. This leads to

$$P_{av} = \frac{1}{T} \int_0^T \lambda v^2 dt \qquad (4.24)$$

where $T = \frac{2\pi}{\omega}$. Then, the average power expressed by $P_{av} = \frac{\lambda V^2}{2}$ reads

$$P_{av} = \frac{1}{2}\left(\frac{\lambda \kappa^2 \omega^2}{(\lambda - \lambda \cos(\omega\tau))^2 + (\omega + \lambda \sin(\omega\tau))^2}\right)a^2 \qquad (4.25)$$

where the amplitude a is obtained from (4.23). Using the maximization procedure, the maximum power response is given by

$$P_{max} = \frac{\lambda \kappa^2 \omega^2 a^2}{(\lambda - \lambda \cos(\omega\tau))^2 + (\omega + \lambda \sin(\omega\tau))^2} \qquad (4.26)$$

Equations (4.23) and (4.26) are used to examine the influence of different system parameters on the periodic response and on the corresponding maximum output power of the harvester.

To approximate the QP response of the original system, we apply the second-step perturbation method [22] on the modulation equations (4.20). To this end, it is convenient to transform the modulation equations (4.20) from the polar form to the following Cartesian system using the variable change $u = a\cos\theta$ and $w = -a\sin\theta$

$$\begin{cases} \dfrac{du}{dt} = S_4 w + \mu\{S_1 u + S_2 u(u^2 + w^2)\} \\[2mm] \dfrac{dw}{dt} = -S_4 u - S_3 + \mu\{S_1 w + S_2 w(u^2 + w^2)\} \end{cases} \qquad (4.27)$$

where μ is a new bookkeeping parameter introduced to perform the second-step multiple scales method. A periodic solution of the slow flow (4.27) corresponding to the QP response of the original system (4.9), (4.10) can be expressed in the forme

$$u(t) = u_0(T_0, T_1) + \mu u_1(T_0, T_1) + O(\mu^2) \qquad (4.28)$$

$$w(t) = w_0(T_0, T_1) + \mu w_1(T_0, T_1) + O(\mu^2) \qquad (4.29)$$

where $T_0 = t$ and $T_1 = \mu t$. The time derivatives become $\frac{d}{dt} = D_0 + \mu D_1 + O(\mu^2)$ where $D_i^j = \frac{\partial^j}{\partial^j T_i}$. Substituting (4.28) and (4.29) into (4.27), and equating coefficient of like powers of μ, we obtain at the first order

$$D_0^2 u_0 + S_4^2 u_0 = -S_3 S_4 \tag{4.30}$$

$$S_4 w_0 = D_0 u_0 \tag{4.31}$$

and at the second order we have

$$D_0^2 u_1 + S_4^2 u_1 = -D_0 D_1 u_0 + S_1 D_0 u_0 + S_2 D_0 u_0 (u_0^2 + w_0^2)$$
$$-S_4 D_1 w_0 + S_2 u_0 D_0 (u_0^2 + w_0^2) + S_4 S_1 w_0 + S_4 S_2 w_0 (u_0^2 + w_0^2) \tag{4.32}$$

$$S_4 w_1 = D_0 u_1 + D_1 u_0 - S_1 u_0 - S_2 u_0 (u_0^2 + w_0^2) \tag{4.33}$$

where S_4 is the frequency of the QP modulation. The solution up to the first order is written as

$$u_0(T_0, T_1) = R(T_1) \cos(S_4 T_0 + \psi(T_1)) - \alpha_2 \tag{4.34}$$

$$w_0(T_0, T_1) = -R \sin(S_4 T_0 + \psi(T_1)) \tag{4.35}$$

where R and ψ are, respectively, the amplitude and the phase of the QP modulation and $\alpha_2 = \frac{S_3}{S_4}$. Substituting (4.34) and (4.35) into (4.32) and removing secular terms gives the following *slow-modulation* equations

$$\begin{cases} \dfrac{dR}{dt} = (S_1 + 2 S_2 \alpha_2^2) R + S_2 R^3 \\[2mm] R \dfrac{d\psi}{dt} = 0 \end{cases} \tag{4.36}$$

The equilibria of this *slow-modulation* system determine the periodic solutions of the modulation equations (4.36), corresponding to the QP solutions of the original system (4.9), (4.10). The nontrivial equilibrium obtained by setting $\frac{dR}{dt} = 0$ is given by

$$R = \sqrt{-\frac{S_1 + 2 S_2 \alpha_2^2}{S_2}} \tag{4.37}$$

Consequently, the approximate periodic solution of the slow flow (4.27) is given by

$$u(t) = R\cos(\theta t) - \alpha_2 \tag{4.38}$$

$$w(t) = -R\sin(\theta t) \tag{4.39}$$

The approximate amplitude $a(t)$ of the QP response reads

$$a(t) = \sqrt{R^2 + \alpha_2^2 - 2\alpha_2 R \cos(\theta t)} \tag{4.40}$$

and the QP modulation envelope is delimited by a_{min} and a_{max} given by

$$a_{min} = min\{\sqrt{R^2 + \alpha_2^2 \pm 2\alpha_2 R}\} \tag{4.41}$$

$$a_{max} = max\{\sqrt{R^2 + \alpha_2^2 \pm 2\alpha_2 R}\} \tag{4.42}$$

The explicit expression of the QP response of the original equation (4.9) is then written as

$$x(t) = u(t)\cos(\omega t) + w(t)\sin(\omega t) \tag{4.43}$$

On the other hand, the QP solution of the voltage $v(t)$, obtained by inserting (4.43) into (4.8), can be extracted via a convolution integral with the boundary condition $v(0) = v(T)$ where $T = \frac{2\pi}{\nu}$. This leads to

$$v(t) = -\kappa e^{(\lambda e^{\lambda \tau} - \lambda)t} \int_0^t \dot{x}(t') e^{(\lambda - \lambda e^{\lambda \tau})t'} dt' \tag{4.44}$$

Consequently, the power, the average and the maximum output powers in the QP regime are given, respectively, by

$$P_{QP}(t) = \lambda(-\kappa e^{(\lambda e^{\lambda \tau} - \lambda)t} \int_0^t \dot{x}(t') e^{(\lambda - \lambda e^{\lambda \tau})t'} dt')^2 \tag{4.45}$$

$$P_{avQP} = \frac{\lambda \kappa^2 \nu^2}{2[(\lambda - \lambda\cos(\omega\tau))^2 + (\nu + \lambda\sin(\omega\tau))^2]} a^2 \tag{4.46}$$

$$P_{maxQP} = \frac{\lambda \kappa^2 \nu^2}{[(\lambda - \lambda\cos(\omega\tau))^2 + (\nu + \lambda\sin(\omega\tau))^2]} a^2 \tag{4.47}$$

where $\nu = S_4$ is the frequency of the QP modulation and a is now derived from (4.41) and (4.42).

Figure 4.8a, b show the frequency response of periodic and QP solutions and the corresponding output power amplitudes (P_{max}, P_{maxQP}) versus the frequency ω, respectively, in the case of the undelayed electrical circuit of the harvester ($\tau = 0$). The periodic response is given by (4.23) and the boundaries of the QP modulation envelope are obtained from (4.41) and (4.42). Similarly, the maximum powers for periodic and QP vibrations are given, respectively, by (4.26) and (4.47). For validation, the analytical prediction (solid lines for stable and dashed line for unstable) are compared to numerical simulation (circles) obtained using Runge Kutta of order 4. The plots in Fig. 4.8b show that in the absence of time delay, periodic vibration-based EH can be achieved, but in a very narrow region located around the resonance peak. Instead, QP vibration-based EH can be obtained over a broadband of frequency

Fig. 4.8 Vibration and
power amplitudes versus ω
for $\alpha = 0.1$, $\beta = 0.2$,
$\chi = 0.05$, $\lambda = 0.05$,
$\kappa = 0.5$, $f = 0.08$ and
$\tau = 0$. Analytical prediction
(solid lines for stable and
dashed line for unstable) and
numerical simulation
(circles)
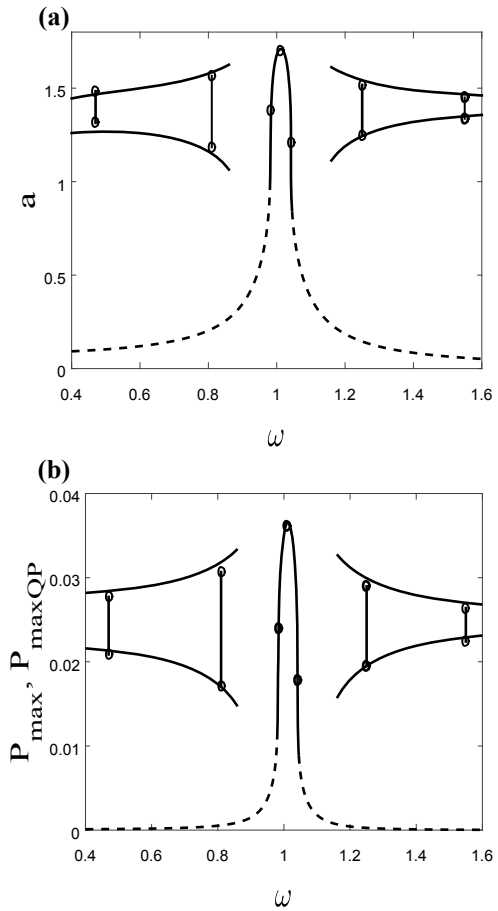
away from the resonance with a performance comparable to that provided by periodic
vibrations.

In Fig. 4.9 is shown the influence of time delay in the electrical component on the
EH performance of the system. The curves given by the *black* lines correspond to
the delayed case ($\tau = 6.2$). For comparison, we plot in *grey* the case where the delay
is absent ($\tau = 0$). It can be observed that the presence of the delay in the electrical
circuit increases the QP output power over a certain range of the frequency ω located
away from the resonance (Fig. 4.9b). This QP output power can achieve a better
performance comparing to the periodic output power, as illustrated in the vicinity of
$\omega = 0.8$ and $\omega = 1.2$ (Fig. 4.9b).

Fig. 4.9 Vibration and power amplitudes versus ω for $\alpha = 0.1$, $\beta = 0.2$, $\chi = 0.05$, $\lambda = 0.05$, $\kappa = 0.5$ and $f = 0.08$. Analytical prediction (solid lines for stable and dashed line for unstable) and numerical simulation (circles). *black* lines for delayed electric circuit ($\tau = 6.2$) and *grey* lines for undelayed circuit ($\tau = 0$, Fig. 4.8)
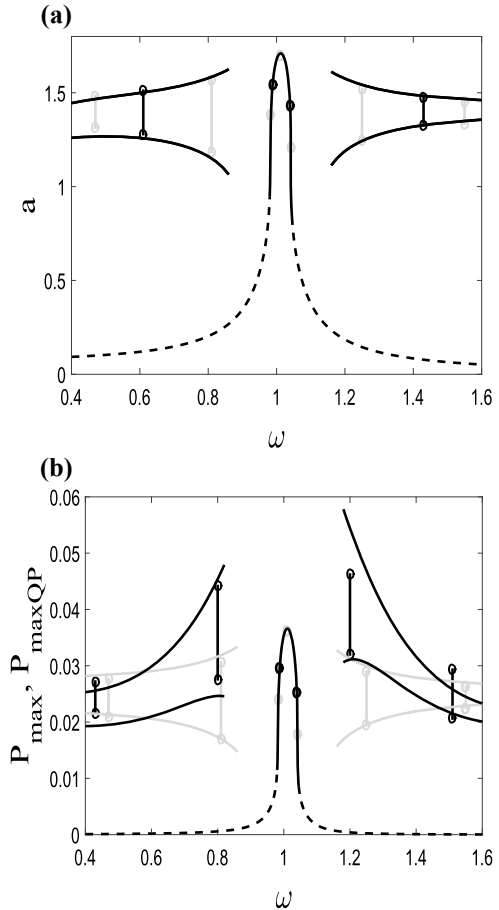
To ensure the stability of the QP vibrations during energy extraction operation, it is important to determine the stability chart of the response. This can be done by considering the stability of the nontrivial solution of the slow-slow flow (4.36) obtained by calculating the eigenvalues of the corresponding Jacobian matrix **J**. The curves delimiting the regions of existence of the QP oscillations and their domains of stability are given by the conditions ($Tr(\mathbf{J}) = -2S_1 - 4S_2\alpha_2^2 < 0$ and $Det(\mathbf{J}) = 0$).

Figure 4.10a shows this stability chart in the parameter plane (f, ω) for $\tau = 6.2$ indicating the *grey* regions where stable QP (SQP) solutions take place and the *white* region corresponding to stable periodic (SP) solutions. In Fig. 4.10b are shown time histories and the corresponding output power responses related to crosses labelled 1, 2, 3 in Fig. 4.10a. From cross 1 to cross 2 or 3 the response bifurcates from SP to SQP oscillations via secondary Hopf bifurcation producing a slight modulation of the amplitude response and a significant performance of the output power at cross 3.
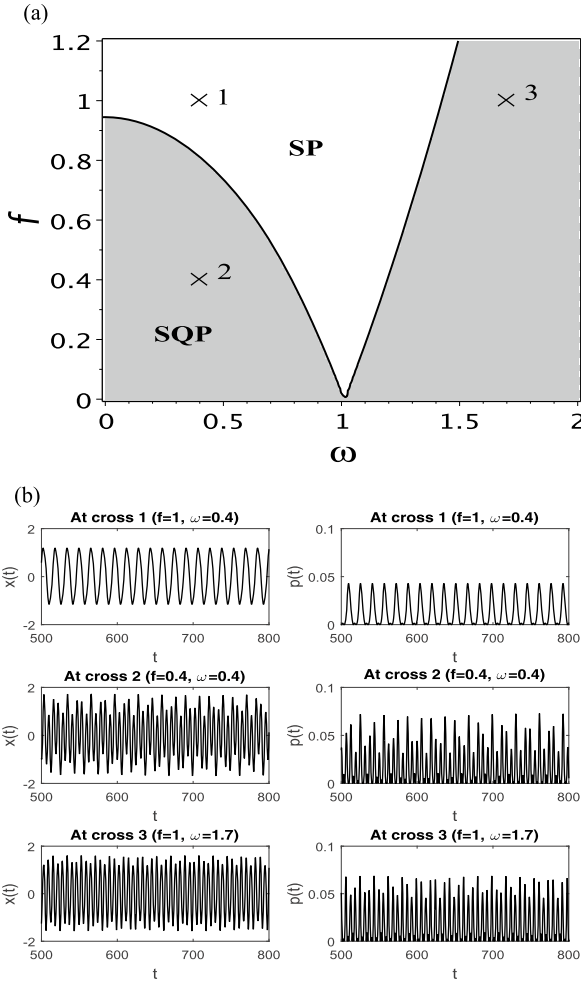
(a)

(b)

Fig. 4.10 **a** Stability chart in the plane (f, ω), **b** time and power histories corresponding to different regions picked from (**a**). SP: stable periodic, SQP: stable QP; $\alpha = 0.1, \beta = 0.2, \chi = 0.05, \lambda = 0.05, \alpha = 0.1, \kappa = 0.5$, and $\tau = 6.2$

Finally, we show in Fig. 4.11 the variation of vibration and maximum power amplitudes χ versus the piezoelectric coupling coefficient χ. It can be seen that a good performance of QP vibration-based EH can be achieved in certain range of negative χ located slightly at the right of the periodic region near $\chi = -0.5$ (Fig. 4.11b).

Fig. 4.11 Vibration and power amplitudes versus χ for $\alpha = 0.1$, $\beta = 0.2$, $\omega = 0.8$, $\lambda = 0.05$, $\alpha = 0.1$, $\kappa = 0.5$ and $f = 0.08$. Analytical prediction (solid lines for stable and dashed line for unstable) and numerical simulation (circles). *black* lines for delayed circuit ($\tau = 6.2$) and *grey* lines for undelayed circuit ($\tau = 0$)
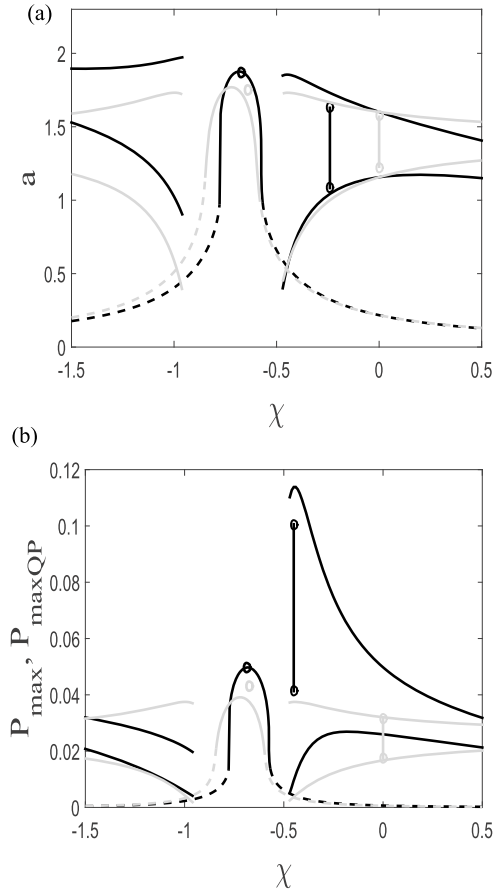
4.4 Conclusions

We have provided in a first part of the chapter recent results in QP vibration-based EH for some variants of delayed van der Pol harvesters for which the delay amplitude is modulated with certain amplitude and frequency around a nominal value. These variants include the delayed van der Pol harvester coupled either to delayed or undelayed electromagnetic subsystem. The influence of delay parameters on the performance of the harvester has been examined. In particular, it was shown that when the delay is introduced in both the mechanical oscillator and the electrical circuit the maximum output power extracted from QP vibrations does not necessarily correspond to the maximum amplitude of QP oscillations.

In a second part of the chapter we have investigated QP vibration-based EH in the case where the van der Pol oscillator is subjected to external harmonic excitation and coupled to a delayed piezoelectric component. The second-step multiple scales

method was applied near the primary resonance to obtain approximation of the QP responses as well as the amplitude of the harvested power. Results showed that in the presence of time delay in the electrical circuit of the harvester, it is possible to harvest energy from the induced QP vibrations with a good performance over a broadband of system parameters away from the resonance. Such a performance is comparable to the one provided by the periodic vibrations, except that the energy extracted from periodic vibrations can be achieved only in a narrow region located around the resonance peak, while energy extracted from QP vibrations can be attained over a broadband of frequency away from the resonance. To guarantee the robustness of the QP vibration during energy extraction operation, a stability analysis was performed and the QP stability chart was determined. Numerical simulations have been conducted to confirm the analytical predictions. This study provides an interesting alternative to harvest energy in nonlinear harvesters away from the resonance, as instabilities and jump phenomena present often difficulty in maintaining energy harvesting operations in a stable and robust regime near the resonance.

References

1. N.G. Stephen, On energy harvesting from ambient vibration. J. Sound Vib. **293**, 409–425 (2006)
2. G.A. Lesieutre, G.K. Ottman, H.F. Hofmann, Damping as a result of piezoelectric energy harvesting. J. Sound Vib. **269**, 991–1001 (2004)
3. H.A. Sodano, D.J. Inman, G. Park, Generation and storage of electricity from power harvesting devices. J. Intell. Mater. Syst. **16**, 67–75 (2005)
4. H.A. Sodano, D.J. Inman, G. Park, Comparison of piezoelectric energy harvesting devices for recharging batteries. J. Intell. Mater. Syst. **16**, 799–807 (2005)
5. D.D. Quinn, A.L. Triplett, A.F. Vakakis, L.A. Bergman, Energy harvesting from impulsive loads using intestinal essential nonlinearities. J. Vib. Acoust. **133**, 011004 (2011)
6. A. Abdelkefi, A.H. Nayfeh, M.R. Hajj, Modeling and analysis of piezoaeroelastic energy harvesters. Nonlinear Dyn. **67**, 925–939 (2011)
7. A. Abdelkefi, A.H. Nayfeh, M.R. Hajj, Design of piezoaeroelastic energy harvesters. Nonlinear Dyn. **68**, 519–530 (2012)
8. B.P. Mann, N.D. Sims, Energy harvesting from the nonlinear oscillations of magnetic levitation. J. Sound Vib. **319**, 515–530 (2009)
9. A. Bibo, M.F. Daqaq, Energy harvesting under combined aerodynamic and base excitations. J. Sound Vib. **332**, 5086–5102 (2013)
10. M. Hamdi, M. Belhaq, Quasi-periodic vibrations in a delayed van der Pol oscillator with time-periodic delay amplitude. J. Vib. Control (2015). https://doi.org/10.1177/1077546315597821
11. M. Belhaq, M. Hamdi, Energy harversting from quasi-periodic vibrations. Nonlinear Dyn. **86**, 2193–2205 (2016)
12. Z. Ghouli, M. Hamdi, F. Lakrad, M. Belhaq, Quasiperiodic energy harvesting in a forced and delayed Duffing harvester device. J. Sound Vib. **407**, 271–285 (2017)
13. Z. Ghouli, M. Hamdi, M. Belhaq, Energy harvesting from quasi-periodic vibrations using electromagnetic coupling with delay. Nonlinear Dyn. **89**, 1625–1636 (2017)
14. M. Belhaq, Z. Ghouli, M. Hamdi, Energy harvesting in a Mathieu-van der Pol-Duffing MEMS device using time delay. Nonlinear Dyn. **94**, 2537–2546 (2018)
15. Z. Ghouli, M. Hamdi, M. Belhaq, Improving energy harvesting in excited Duffing harvester device using a delayed piezoelectric coupling, in *MATEC Web of Conferences*, vol. 241 (2018), pp. 01010

16. I. Kirrou, A. Bichri, M. Belhaq, Energy harvesting in a delayed Rayleigh harvester device, in *MATEC Web of Conferences*, vol. 241 (2018), pp. 01026
17. G. Stepan, T. Kalmr-Nagy, Nonlinear regenerative machine tool vibrations, in *Proceedings of the 1997 ASME Design Engineering Technical Conferences, 16th ASME Biennial Conference on Mechanical Vibration and Noise (Sacramento, 1997)*, DETC97/VIB-4021 (1997), pp. 1–11
18. T. Kalmr-Nagy, G. Stepan, F.C. Moon, Subcritical Hopf bifurcation in the delay equation model for machine tool vibrations. Nonlinear Dyn. **26**, 121–142 (2001)
19. R. Rusinek, A. Weremczuk, J. Warminski, Regenerative model of cutting process with nonlinear Duffing oscillator. Mech. Mech. Eng. **15**, 129–143 (2011)
20. A.H. Nayfeh, D.T. Mook, *Nonlinear Oscillations* (Wiley, New York, 1979)
21. L.E. Shampine, S. Thompson, Solving delay differential equations with dde23 (2000). http://www.radford.edu/~thompson/webddes/tutorial.pdf
22. M. Belhaq, M. Houssni, Quasi-periodic oscillations, chaos and suppression of chaos in a nonlinear oscillator driven by parametric and external excitations. Nonlinear Dyn. **18**, 1–24 (1999)